





Manganese promotes α -synuclein amyloid aggregation through the induction of protein phase transition

Received for publication, July 23, 2021, and in revised form, November 24, 2021 Published, Papers in Press, December 4, 2021, <https://doi.org/10.1016/j.jbc.2021.101469>

Bingkuan Xu¹, Shuai Huang¹, Yinghui Liu^{1,*}, Chun Wan², Yuanyuan Gu³, Dianliang Wang^{4,*} , and Haijia Yu^{1,*} 

From the ¹Jiangsu Key Laboratory for Molecular and Medical Biotechnology, College of Life Sciences, Nanjing Normal University, Nanjing, China; ²Department of Molecular, Cellular and Developmental Biology, University of Colorado, Boulder, Colorado, USA; ³Medical Safeguard Center, and ⁴Stem Cell and Tissue Engineering Research Laboratory, PLA Rocket Force Characteristic Medical Center, Beijing, China

Edited by Paul Fraser

α -Synuclein (α -Syn) is the major protein component of Lewy bodies, a key pathological feature of Parkinson's disease (PD). The manganese ion Mn^{2+} has been identified as an environmental risk factor of PD. However, it remains unclear how Mn^{2+} regulates α -Syn aggregation. Here, we discovered that Mn^{2+} accelerates α -Syn amyloid aggregation through the regulation of protein phase separation. We found that Mn^{2+} not only promotes α -Syn liquid-to-solid phase transition but also directly induces soluble α -Syn monomers to form solid-like condensates. Interestingly, the lipid membrane is integrated into condensates during Mn^{2+} -induced α -Syn phase transition; however, the preformed Mn^{2+} / α -syn condensates can only recruit lipids to the surface of condensates. In addition, this phase transition can largely facilitate α -Syn amyloid aggregation. Although the Mn^{2+} -induced condensates do not fuse, our results demonstrated that they could recruit soluble α -Syn monomers into the existing condensates. Furthermore, we observed that a manganese chelator reverses Mn^{2+} -induced α -Syn aggregation during the phase transition stage. However, after maturation, α -Syn aggregation becomes irreversible. These findings demonstrate that Mn^{2+} facilitates α -Syn phase transition to accelerate the formation of α -Syn aggregates and provide new insights for targeting α -Syn phase separation in PD treatment.

α -Synuclein (α -Syn), a cytoplasmic protein abundant in presynaptic nerve terminals, is implicated in Parkinson's disease (PD), dementia with Lewy bodies, and other synucleinopathies (1–3). While α -Syn monomer is unstructured and has the potential to form amyloid aggregates (4–6), multiple studies suggested that it forms α -helical tetramers physiologically that resist aggregation (7, 8). α -Syn is involved in neurotransmitter release and many other critical membrane trafficking processes. However, its physiological function has not been completely understood (9). In PD, α -Syn forms oligomeric and fibrillar aggregates through the intermolecular assemblies (10, 11). The Lewy bodies and Lewy neurites in the

cytoplasm of neurons are mainly composed of aggregated α -Syn (12, 13). While monomeric α -Syn is soluble and not toxic, numerous studies disclose that α -Syn amyloid oligomers and fibrils are the major causes of cellular toxicity (14, 15). Many cellular pathway alternations, such as oxidative stress, mitochondrial dysfunction, endoplasmic reticulum stress, synaptic dysfunction, and autophagy-lysosomal pathway dysfunction, have been linked to the cytotoxic effects of α -Syn aggregates (15–18).

The aggregations of α -Syn and other amyloid proteins, such as A β , tau, IAPP, FUS, and TDP-43, have been studied *in vivo* and *in vitro* for decades (10, 19, 20). Protein aggregation and amyloid formation are potential targets for amyloid-related disease (10, 16, 17, 21, 22). In addition to α -Syn, the Lewy bodies also contain other cellular components, including various organelles and lipids (20, 23). Many factors, such as proteins and lipids, coexist with α -Syn and affect its accumulation and cellular toxicity (20). For example, the activity of glucocerebrosidase, a lysosomal glycoprotein found in Lewy bodies, affects lipid levels and α -Syn amyloid aggregation (24). Recent studies with Raman spectral imaging revealed that α -Syn fibrils colocalized with lipids in cells (25), while regulations of α -Syn aggregations by lipids have been previously demonstrated (26–28).

Metal ions such as Cu^{2+} , Zn^{2+} , and Mn^{2+} are concentrated in the brain and bind to α -Syn (29). The C-terminal domain of α -Syn, which contains multiple Asp and Glu residues, can interact with many di- and trivalent metal ions (10, 30). However, the detailed information for each metal- α -Syn binding is still unclear due to the lack of high-resolution structure data. Manganese is an essential metal involved in many physiological processes (31, 32). However, the rise of manganese utility in the industry has led to increased manganese pollution. The imbalance of manganese homeostasis has the potential to cause neurodegenerative diseases (33, 34). Specially, epidemiological investigations indicate that excessive exposure to manganese increases the risk of PD (34–36). Multiple studies demonstrated that occupational manganese exposure during welding, mining, and other related industrial activities is associated with Parkinsonism (37–44). Long-time environmental exposure to the high level of air manganese

* For correspondence: Yinghui Liu, yinghui.liu@njnu.edu.cn; Dianliang Wang, wangdianliang@sina.com; Haijia Yu, yuhaijia@njnu.edu.cn.

Mn²⁺-induced α -synuclein phase transition

may also cause deficits of cognitive function (45, 46). A recent meta-analysis based on previous 22 studies revealed a significantly increased level of circulating manganese in PD patients, further demonstrating that manganese level is a potential risk factor for PD (47). One critical cause of neurotoxicity induced by manganese exposure is the increased α -Syn expression and aggregation (48–52). However, most of these studies were based on cell culture, and their relevance to PD is unknown. Biochemical studies showed that manganese not only shortens the aggregation time of α -Syn but also promotes the formation of large fibrillar aggregates (53). However, how manganese promotes α -Syn assembly in the early stage remains elusive.

Many protein–protein or protein–RNA assemblies can form condensed liquid droplets through weak multivalent interactions, called liquid–liquid phase separation (LLPS). Proteins that can undergo LLPS, such as FUS, TDP-43, and Tau protein, usually contain repetitive domains or intrinsically disordered regions (IDR) (54–57). Numerous studies identified that a variety of amyloid aggregation-prone proteins initiate aggregations through LLPS (58–61). α -Syn has three IDRs and multiple low-complexity domains. Recent studies reported that α -Syn undergoes LLPS to accelerate its intermolecular aggregation, indicating that the phase separation could be an early intermediate stage before fibrillar aggregation (62–64).

In this work, we examined whether Mn²⁺ regulates α -Syn through LLPS. We observed that α -Syn undergoes LLPS *in vitro* with the requirement of crowding agents. The addition of Mn²⁺ efficiently promotes α -Syn liquid-to-solid phase transition, facilitating its amyloid aggregation. Interestingly, Mn²⁺ could induce α -Syn monomers to form solid-like condensates directly in the absence of crowding agents, bypassing the step of LLPS. We found that Mn²⁺ could still induce α -Syn phase transition in the presence of lipid membrane. Lipids could be integrated during the formation of condensates but only be recruited to the surface of preformed Mn²⁺/ α -syn condensates. Our studies also demonstrated that Mn²⁺-induced solid-like condensates proceed with aggregations through recruitment of soluble α -Syn monomers. While it is difficult to disassemble the mature α -Syn fibrillar aggregates, our studies showed that metal chelators could reverse Mn²⁺-induced aggregates during the phase transition stage. These findings provide a new dimension for understanding the pathogenesis of manganese-induced PD and suggest that LLPS could be a potential target for PD therapy.

Results

Mn²⁺ promotes α -Syn liquid-to-solid phase transition

To study the regulatory effects of Mn²⁺ on the LLPS of α -Syn, we expressed the full-length human α -Syn (Fig. S1) and examined the conditions in which α -Syn drives LLPS *in vitro*. We first labeled α -Syn by preparing the EGFP- α -Syn fusion protein. The labeled α -Syn and unlabeled α -Syn were mixed at a molar ratio of 1:9 to form liquid droplets (62). Using

fluorescence microscopy, we discovered that α -Syn underwent LLPS with the requirement of a relatively high protein concentration (Fig. S2) and in the presence of crowding agent PEG-10000 (Fig. S3). Ficoll 400, another macromolecular crowding agent, could also promote α -Syn LLPS, although the efficiency is lower (Fig. S4). By contrast, α -Syn failed to drive LLPS in the presence of small-molecule ethylene glycol, supporting that PEG-10000 acts as a crowding agent to drive α -syn LLPS (Fig. S5).

Next, we tested whether Mn²⁺ plays a role in α -Syn LLPS. In the presence of PEG, a frequently used agent to mimic a crowded cellular environment, 200 μ M α -Syn formed the typical smooth liquid droplets. When we included 2 mM Mn²⁺, the morphology of condensates turned irregular (Fig. 1A). The dose-dependence experiments showed that α -syn could form solid-like condensates when Mn²⁺ concentration was 400 μ M or above (Fig. S6). Then we performed fluorescence recovery after photobleaching (FRAP) experiments to further examine the phase of α -Syn condensates. In the absence of Mn²⁺, the fluorescence intensity of α -Syn condensates completely returned to their prebleaching state during the 120 s after laser bleaching, indicating the rapid fluidity of α -Syn inside the droplets (Fig. 1, B and C). In contrast, a dramatic decrease in FRAP with Mn²⁺ was observed in the irregularly shaped aggregates. The fluorescence intensity recovers less than 20% during the 120 s after bleaching either in large or small irregular aggregates (Figs. 1, B and C and S7). These data suggested that the molecular diffusion of protein inside the α -Syn condensates becomes slower, indicating a liquid-to-solid phase transition occurred in the presence of Mn²⁺.

To exclude the effect of EGFP, we used rhodamine (Rhod)-labeled α -Syn to replace EGFP- α -Syn in the LLPS reactions. Similar morphology changes and FRAP results were observed, demonstrating that the labeling fluorophore affects neither the α -Syn LLPS nor the interaction between Mn²⁺ and α -Syn (Fig. S8). These data indicated that Mn²⁺ interacts with α -Syn liquid condensates and efficiently induces a liquid-to-solid transition. Protein self-assembly could be modulated by experimental conditions, which may regulate protein phase separation (10, 61). We then tested the effect of Mn²⁺ on α -Syn phase transition under different conditions. Mn²⁺ could induce the irregular α -syn condensates when we changed the salt concentration or switched to phosphate buffer from Tris. By contrast, Mn²⁺ failed to change α -syn morphology at low pH (5.4) (Fig. S9).

To test whether this α -Syn phase transition is unique to Mn²⁺, we examined the effects of other metal ions on α -Syn LLPS. In the presence of PEG-10000, the sizes of α -Syn droplets increased obviously when Cu²⁺, Zn²⁺, Al³⁺, Ni²⁺, Co²⁺, or Cr²⁺ was individually added (Fig. S10). However, we did not observe irregular condensates in any of these reactions. When we included Mo⁵⁺, α -Syn LLPS was completely inhibited, which might be due to the disruption of the local charge balance (Fig. S10). While the effects of other metal ions need to be further studied, our data support that Mn²⁺-induced quick

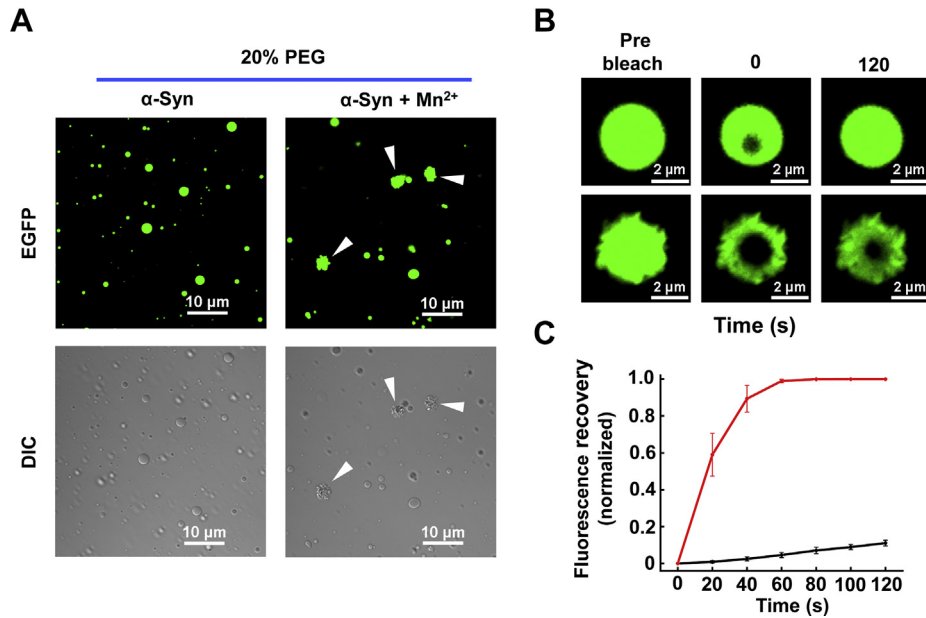


Figure 1. Mn²⁺ promotes α -Syn liquid-to-solid phase transition in the presence of crowding agents. *A*, fluorescence and DIC images showing the formation of EGFP-labeled α -Syn phase-separated condensates in the absence or presence of 2 mM Mn²⁺. The total α -Syn concentration is 200 μ M. *B*, representative FRAP images of α -Syn droplets (*Top*) and Mn²⁺-induced α -Syn condensates (*Bottom*). The fluorescence images of prebleached, bleached (0 s), and bleached after 120 s recovery are shown. *C*, the normalized FRAP curves of α -Syn droplets (*Red*) and Mn²⁺-induced α -Syn condensates (*Black*) shown in (*B*). Data are presented as mean \pm SD (n = 3 independent replicates). All the experiments were carried out in the presence of 20% PEG-10000.

formation of irregular condensates is unique and distinct to the effects of most other metal ions.

Mn²⁺ induces the formation of α -Syn solid-like condensates from soluble monomers

Next, we examined how Mn²⁺ regulates α -Syn phase separation in the absence of crowding agents. α -Syn itself did not undergo LLPS in our conditions without a crowding agent.

Interestingly, when we included Mn²⁺, α -Syn was induced to form phase-separated condensates (Fig. 2A). Based on a dose-dependent experiment, we observed that α -syn started to form phase-separated condensates when Mn²⁺ concentration was 400 μ M (Fig. S11). Little fluorescence recovered in the FRAP experiments of large and small condensates confirmed that the structure of Mn²⁺-induced aggregates is more solid-like (Figs. 2, B and C and S12). These data suggested that Mn²⁺- α -Syn interaction may bypass the stage of LLPS and induce α -

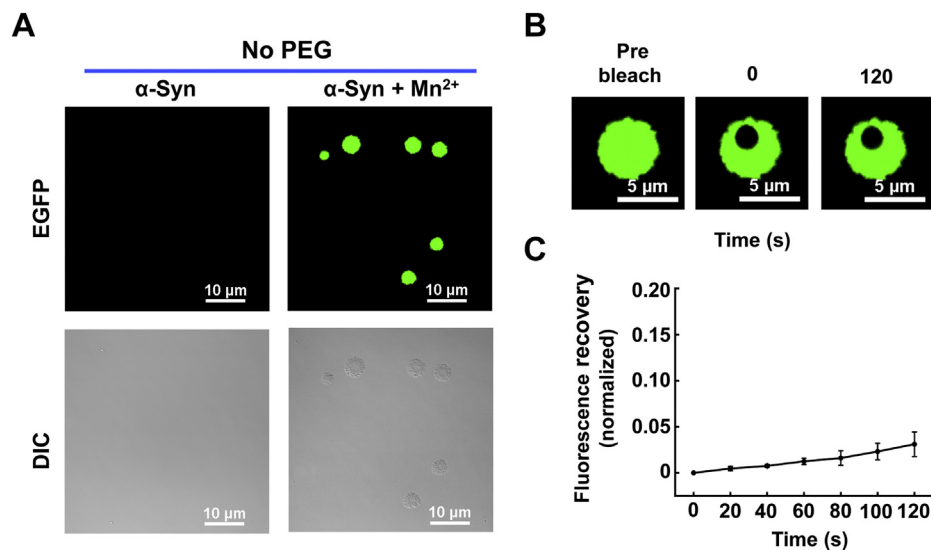


Figure 2. Mn²⁺ induces α -Syn to form solid-like condensates in the absence of crowding agents. *A*, fluorescence and DIC images showing the formation of α -Syn phase-separated condensates in the absence or presence of 2 mM Mn²⁺. The total α -Syn concentration is 200 μ M. *B*, the FRAP images of α -Syn condensates induced by 2 mM Mn²⁺. *C*, the normalized FRAP curves of α -Syn solid-like condensates induced by 2 mM Mn²⁺ under no PEG condition. Data are presented as mean \pm SD (n = 3 independent replicates). All the experiments were performed in the protein storage buffer without PEG.

Mn²⁺-induced α -synuclein phase transition

Syn to a solid-like state directly. Together, our studies indicated that Mn²⁺ could interact with both the soluble α -Syn monomers and liquid phase-separated α -Syn to generate solid-like condensates.

Mn²⁺ induces the irregular α -Syn condensates in the presence of lipid membrane

α -Syn binds to the surface of various lipid membranes, especially the synaptic vesicles (28, 65). Vesicles containing negatively charged lipids can induce α -Syn to form a highly helical structure (66, 67). Lipid membranes were also reported to modulate the formation of amyloid oligomers and fibrils (26–28). It is necessary to test if Mn²⁺ induces α -Syn phase transition in the membrane environment. As crowding agents usually cause liposome clustering, we performed these experiments in the absence of PEG. Our data showed that Mn²⁺ still induced the irregular α -Syn condensates in the presence of liposomes (Fig. 3). Furthermore, the lipid membrane was recruited into α -Syn condensates, indicated by the colocalization of Rhod-labeled lipids (Fig. 3). Interestingly, when we added liposomes to the preformed Mn²⁺/ α -Syn condensates, the lipid membrane could not be integrated into the

condensates. Instead, the fluorescence-labeled lipid membrane is associated with the surface of those Mn²⁺-induced α -Syn condensates (Fig. 3).

Mn²⁺ accelerates the amyloid aggregation of phase-separated α -Syn

As a risky factor of PD, manganese was proposed to promote α -Syn accumulation and cause neurotoxicity. We speculate that Mn²⁺ accelerates α -Syn aggregation through protein phase separation, which can be measured by turbidity and sedimentation assays (68, 69). In the presence of PEG, we observed that α -Syn itself caused high turbidity due to the formation of phase-separated liquid droplets (Fig. 4A) (68). When we included Mn²⁺, a noticeable increase in turbidity was observed. By a sedimentation assay, we can separate the phase-separated α -Syn in pellets from the supernatant (69). We found that Mn²⁺ enhanced the fraction of α -Syn protein recovered from the condensed phase in pellets (Fig. 4B). These data suggested that Mn²⁺ remarkably increases the total amounts of phase-separated α -Syn.

Next, we tested if Mn²⁺-driven α -Syn phase transition accelerates the process of amyloid aggregations. We used

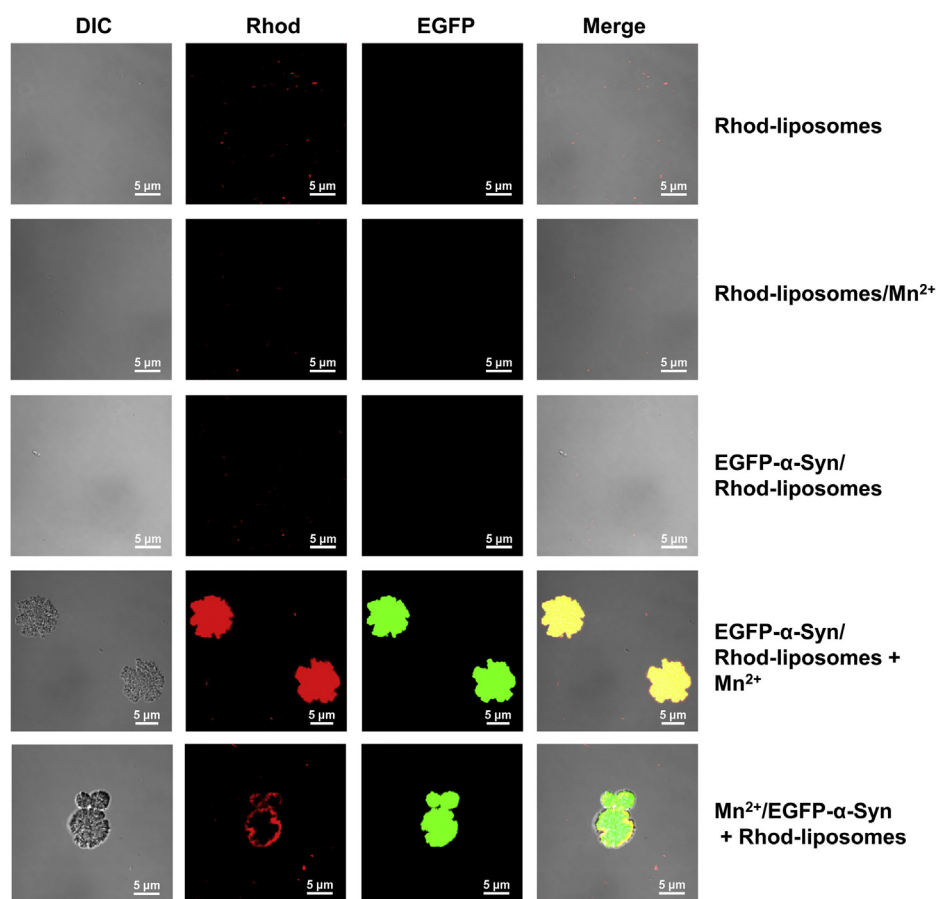


Figure 3. Mn²⁺ induces the irregular α -Syn condensates in the presence of liposomes. Fluorescence and DIC images showing no condensates formed in liposomes alone, liposomes/Mn²⁺, or α -Syn/liposomes. α -Syn were labeled by EGFP, while the liposomes contained 15% PS and were labeled by rhodamine-PE. When α -Syn/liposomes were mixed with Mn²⁺ (α -Syn/liposomes + Mn²⁺), Mn²⁺ induces irregular condensates containing both EGFP-labeled α -Syn and rhodamine-labeled lipids. However, when we added liposomes to the preformed Mn²⁺/ α -Syn, lipids were recruited to the surface of condensates but could not enter the inside. All the experiments were performed in the protein storage buffer without PEG.

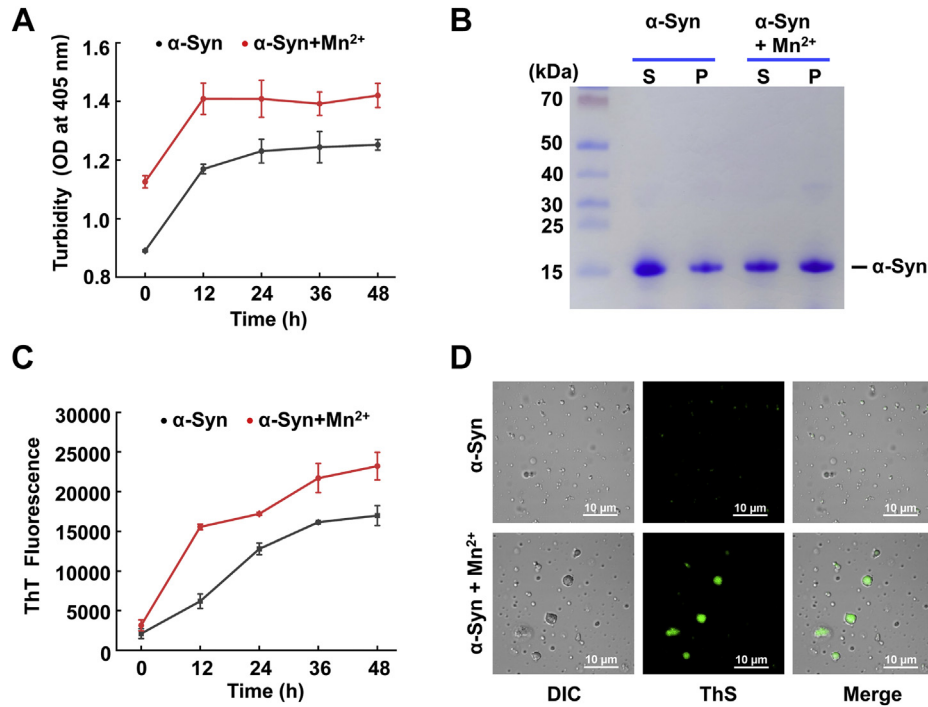


Figure 4. Mn²⁺ increases the amounts of phase-separated α -Syn and facilitates the formation of amyloid aggregates under 20% PEG. *A*, turbidity assays showing the effect of Mn²⁺ on the formation of phase-separated α -Syn. Turbidity was evaluated by monitoring the absorbance at 405 nm, reflecting the amounts of phase-separated protein. Data are presented as mean \pm SD ($n = 3$). *B*, sedimentation-based assays showing the distributions of α -Syn in the supernatant (S) and pellet (P) in the presence and absence of Mn²⁺. *C*, the formation of α -Syn amyloid aggregates indicated by the enhanced ThT fluorescence at 485 nm. Data are presented as mean \pm SD ($n = 3$). *D*, ThS staining assays showing the presence of amyloid structure inside the α -Syn solid-like condensates induced by Mn²⁺. α -Syn condensates were incubated with ThS for 12 h before the observations. ThS copartitioning inside the Mn²⁺-treated α -Syn condensates indicates the formation of amyloid structure.

Thioflavin T (ThT), a specific fluorescence dye for aggregated amyloid, to detect the α -Syn aggregation in solution (70). Mn²⁺ largely enhanced the ThT fluorescence, suggesting that it turns α -Syn toward amyloid aggregates (Fig. 4C). This Mn²⁺-facilitated α -Syn amyloid-like aggregation was further confirmed by Thioflavin S (ThS) staining, which showed concentrated ThS fluorescence in the larger solid-like condensates (Fig. 4D). We then examined the cytotoxicity of Mn²⁺-induced α -Syn condensates using rat pheochromocytoma PC12 cells by the MTT method. α -Syn monomers or Mn²⁺ individually had little or slight cellular toxicity on PC12 cells, consistent with previous reports (Fig. S13) (51, 71). When we added Mn²⁺-induced α -Syn condensates, the cell viability decreased obviously (Fig. S13). The cytotoxicity of Mn²⁺-induced α -Syn condensates is comparable to the preformed α -Syn or Mn²⁺/ α -Syn fibril (Fig. S13), indicating that Mn²⁺- α -Syn interaction facilitates the formation of toxic α -Syn aggregates. Together, our data suggested that Mn²⁺ facilitates α -Syn liquid-to-solid state transition to accelerate amyloid aggregation.

Mn²⁺-induced α -Syn condensates do not fuse but recruit soluble α -Syn monomers

The phase-separated protein droplets during LLPS are usually able to fuse (72, 73). Using α -Syn liquid droplets labeled with different fluorophores, we observed that the universal α -Syn liquid droplets fusion occurred in the presence of PEG (Fig. S14). Next, we tested if Mn²⁺-involved α -Syn

condensates keep the ability to fuse. Since all the α -Syn condensates formed without PEG are purely generated by Mn²⁺-protein interaction, we chose to study the fusion activity of Mn²⁺-induced condensates in the absence of crowding agents. EGFP- and Rhod-labeled α -Syn forms fluorescent α -Syn condensates in the presence of Mn²⁺, respectively (Fig. 5). When we mixed these preformed α -Syn condensates, no fusion was observed (Fig. 5). Interestingly, when we added Rhod-labeled α -Syn monomers into preformed Mn²⁺/EGFP- α -Syn condensates, the monomers were integrated inside the condensates freely (Fig. 5). Thus, the Mn²⁺-induced α -Syn condensates lose the ability to fuse because of their more rigid solid-like structures. However, Mn²⁺ does not block the recruitment of α -Syn monomers. These data further indicated that Mn²⁺-induced α -Syn condensates are not entirely solidified in the early stage and may serve as an intermediate stage toward mature amyloid aggregates.

Mn²⁺-induced α -Syn phase transition is reversible

Metal ion–protein interactions could usually be reversed by chelators. Next, we examined whether Mn²⁺-induced α -Syn phase transition is reversible. The addition of EDTA, a commonly used metal ion chelating agent, efficiently eliminated the Mn²⁺-induced condensates in the absence of PEG-10000. When excess Mn²⁺ was added, α -Syn condensates reformed. The formation of α -Syn condensates was regulated by excess Mn²⁺ or EDTA in the reaction, indicating that this

Mn²⁺-induced α -synuclein phase transition

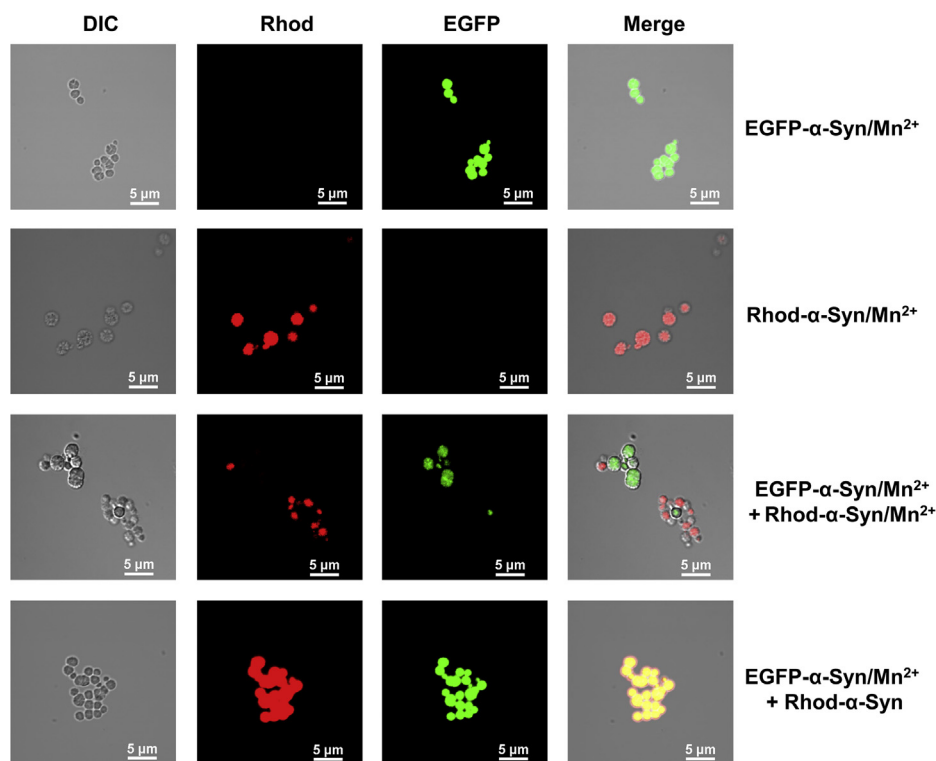


Figure 5. Mn²⁺-induced α -Syn condensates do not fuse but recruit α -Syn monomers. Representative images of EGFP-labeled α -Syn condensates (EGFP-labeled α -Syn/Mn²⁺), Rhod-labeled α -Syn condensates (Rhod-labeled α -Syn/Mn²⁺) showing the formation of α -Syn solid-like condensates labeled with different colors. The two condensates did not fuse (EGFP-labeled α -Syn/Mn²⁺ + Rhod-labeled α -Syn/Mn²⁺) when they were mixed. However, when the Rhod-labeled α -Syn monomers were added to EGFP-labeled α -Syn condensates, they were merged into the condensates (EGFP-labeled α -Syn/Mn²⁺ + Rhod-labeled α -Syn). All the experiments were performed in the protein storage buffer without PEG.

process is highly reversible (Fig. 6A). Further experiments with the turbidity assay showed that Mn²⁺ and EDTA reversibly control the phase-separated protein accumulations, supporting the conclusion that α -Syn phase transition induced by Mn²⁺ is reversible (Fig. 6B). We then tested whether Mn²⁺-induced irregular condensates can be reversed back to the liquid droplets. When Mn²⁺ was chelated by EDTA, we observed the universal liquid droplets but no irregular condensates in the presence of PEG (Fig. S15). EDTA decreased the turbidity of Mn²⁺-treated α -Syn to the Mn²⁺-untreated level, further demonstrating that EDTA reverses the Mn²⁺-induced solid-like condensates back to liquid droplets (Fig. S15). However, once the fibrillar aggregates matured, EDTA could not reverse α -Syn aggregation (Fig. S16). Together, these data clearly showed that Mn²⁺-induced α -Syn aggregation is reversible at the early stage of phase transition but irreversible after the fibrillar aggregates matured.

Discussion

Accumulation of α -Syn in Lewy bodies is the pathological hallmark of PD. Conversion of soluble α -Syn into fibrillar aggregates is the central event in the process. Excessive manganese can cause neurotoxicity and increase the risk of PD. Manganese leads to α -Syn overexpression and accumulation inside the cell and facilitates its cell-to-cell transmission (51, 52). However, the molecular mechanism of α -Syn aggregations regulated by Mn²⁺ remains unclear.

LLPS is involved in multiple cellular and pathophysiological processes. For example, FUS initiates DNA damage repair through LLPS, and abnormal phase separation of TDP-43 can cause neuron cell death (56, 74). α -Syn undergoes LLPS to form condensates, acting as an intermediate to initiate fibrillar aggregations (62). The phase transition during α -Syn accumulation could be a potential target for PD and other synucleinopathies. Fe³⁺ and Cu²⁺ were recently shown to promote α -Syn LLPS by accelerating the formation of liquid droplets (62). In this study, we showed that various metal ions, including Cu²⁺, Zn²⁺, Al³⁺, Ni²⁺, Co²⁺, and Cr²⁺, modulated α -Syn LLPS by enlargement of the liquid droplets. By contrast, Mn²⁺ dramatically induced the irregular α -Syn condensates by facilitating the liquid-to-solid phase transition of preformed α -Syn droplets. Besides, Mn²⁺ was able to drive α -Syn monomers to form solid-like condensates directly. While most of these heavy metal ions promote α -Syn aggregation, our studies suggested that they may take diverse mechanisms. The Mn²⁺-induced phase transition facilitated α -Syn intermolecular assembly and accelerated the amyloid aggregation (Fig. 6C).

However, the induction of irregular α -syn condensates requires an excess of Mn²⁺. Our data indicated that the irregular condensates appear only when the molar ratio of Mn²⁺/ α -syn reaches 2 or above. We assume a high Mn²⁺/ α -syn ratio requirement is due to the low binding affinity between them (30, 75). It is known that Mn²⁺ interacts with α -syn primarily through the C-terminal residues of the protein (10, 30).

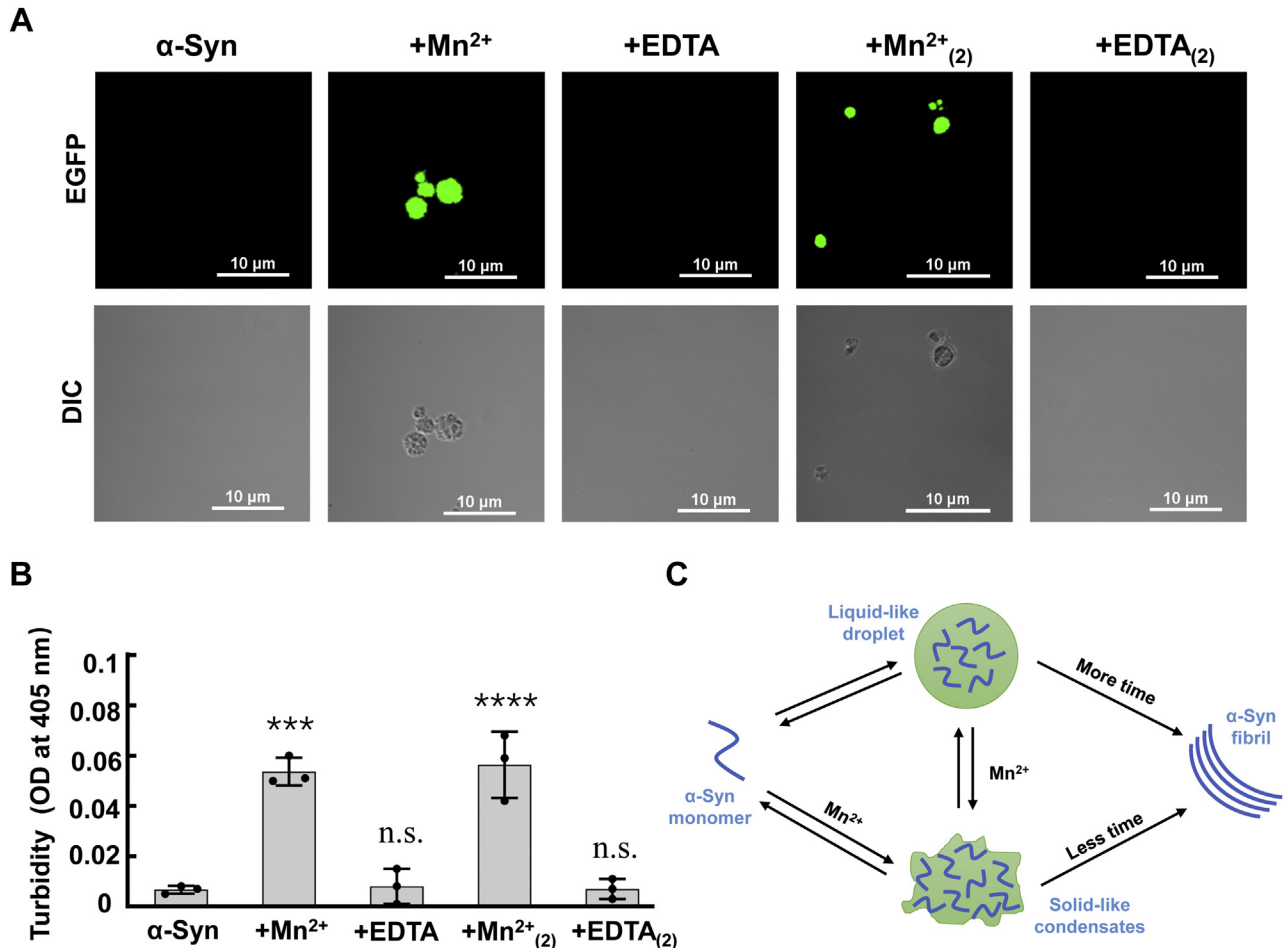


Figure 6. Mn²⁺-induced α -Syn solid-like condensates can be reversed by metal chelators. *A*, fluorescence and DIC images showing the formation of α -Syn solid-like condensates was circularly controlled by excess Mn²⁺ or EDTA in the reaction. The excess concentration of Mn²⁺ or EDTA was 2 mM or 0.5 mM in each round. *B*, turbidity measurements of the samples shown in (*A*). Data are presented as mean \pm SD (n = 3). *p* values were calculated using one-way ANOVA with Tukey's multiple comparisons test. n.s., *p* > 0.05. ****p* < 0.001. *****p* < 0.0001. The calculated *p* values for +Mn²⁺, +EDTA, +Mn²⁺₍₂₎, +EDTA₍₂₎ were ****p* = 0.0001, n.s., *p* = 0.9994, *****p* < 0.0001, n.s., *p* > 0.9999. *C*, schematic illustration showing α -Syn undergoes phase transitions to form fibrillar aggregation in the absence or presence of Mn²⁺.

However, the detailed binding information is still lacking. The high-resolution structural insights are required to illustrate the mechanisms of how Mn²⁺ interacts with α -syn to induce phase transition and amyloid aggregation. The correlation between our biochemical study and manganese exposure caused PD, which also needs to be further examined.

Mn²⁺ induces α -syn phase transition in the presence of lipid membrane, which is another interesting finding. Importantly, the Mn²⁺/ α -syn condensates can recruit the lipids from vesicles, consistent with previous findings that lipids colocalize with α -syn fibrils in Lewy bodies (23). One of the characteristics of liquid droplets during LLPS is they can fuse (72). We observed that although wide-type α -Syn liquid droplets can easily fuse, the Mn²⁺-induced α -Syn condensates could not fuse at all. However, these solid-like condensates keep the ability to recruit soluble α -Syn monomers to enlarge the aggregates.

The aggregation of α -Syn serves as a promising target for PD therapies, and this strategy has been extensively studied for many years (16, 22, 76). Successful drug candidates may target any of the stages during α -Syn aggregation. As for the

treatment of Mn²⁺-caused α -Syn accumulation, it is critical to figure out in which stage metal chelators can reverse α -Syn aggregation. We discovered that EDTA could not efficiently reduce the amyloid aggregation once Mn²⁺- α -Syn aggregates matured. Interestingly, the protein aggregation could be reversed by chelators at the early stage of Mn²⁺-induced phase transition. Our studies suggested that phase transition is a promising target for Mn²⁺-caused α -Syn accumulations in PD. As other factors that modulate α -Syn aggregations have the possibilities to regulate LLPS as well, the phase transition of α -Syn could be a general key target for PD treatment. In support of this, recent studies have reported that protein LLPS can be modulated by small molecules, either inducing or preventing the formation of liquid droplets (77, 78).

Taken together, these findings suggest that Mn²⁺ promotes α -Syn amyloid aggregation through the stage of early LLPS. Mn²⁺ interacts with α -Syn, alters the pathway of LLPS by facilitating the liquid-to-solid phase transition or directly inducing the solid-like condensates (Fig. 6C). Metal manganese exposure is a risk factor for PD by increasing α -Syn accumulations. Our study establishes the molecular mechanism

Mn²⁺-induced α -synuclein phase transition

by which Mn²⁺ promotes α -Syn amyloid aggregation, revealing that the early phase transition could be a future target for PD therapies.

Experimental procedures

Protein expression and purification

Recombinant untagged α -Syn was expressed in *Escherichia coli* and purified by nickel affinity chromatography, using a previously established procedure (79–82). The human α -Syn gene was cloned into a pET28a-based SUMO vector. His6-SUMO- α -Syn fusion protein was digested by SUMO proteases to remove the extra His6-SUMO tags. The untagged α -Syn protein was purified using gel filtration chromatography and subsequently dialyzed overnight against a protein storage buffer (25 mM Tris-HCl [pH7.4], 50 mM NaCl). To prepare the EGFP- α -Syn protein, EGFP and α -Syn coding sequences were incorporated together into a pET28a-based SUMO vector, and the fusion protein was generated following the same procedure as α -Syn.

Protein labeling

α -Syn was fluorescence-labeled by a rhodamine labeling kit following the manufacturer's instructions (Thermo Fisher Scientific). Briefly, the α -Syn protein was dialyzed against the labeling buffer (50 mM sodium borate, pH 8.5) and mixed with 15-fold molar excess of rhodamine dye. After incubation at room temperature for 1 h, the excess dye was removed by overnight dialysis against the protein storage buffer.

The labeling degree of α -Syn with rhodamine dye was calculated following the manufacturer's instructions.

First, we calculated the concentration of the protein in the sample using the equation:

$$\text{Protein concentration (M)} = \frac{A_{280} - (A_{\text{max}} \times \text{CF})}{\epsilon}$$

Where CF = Correction factor. The CF of rhodamine dye is 0.34, provided by the manufacturer's instructions. ϵ = protein molar extinction coefficient, $\epsilon_{\alpha\text{-Syn}}$ is 5960 M⁻¹ cm⁻¹. A_{max} = Absorbance value of the protein-dye conjugate measured at the wavelength maximum of dye. A_{280} = Absorbance value of protein-dye conjugate measured at 280 nm.

Then, the degree of labeling was calculated by the following equation:

$$\text{Moles dye per mole protein} = \frac{A_{\text{max}} \text{ of the labeled protein}}{\epsilon' \times \text{protein concentration (M)}}$$

Where ϵ' = molar extinction coefficient of the fluorescent dye.

We calculated the labeling ratio as 0.77 \pm 0.15 mol dye per mole protein in our α -Syn protein labeling experiment.

In vitro formation of α -Syn condensates

The formation of α -Syn condensates was performed in the presence of the crowding agent PEG-10000. Unlabeled α -Syn and fluorescence-labeled α -Syn were mixed at a molar ratio of

9:1. 200 μ M α -Syn mixture was incubated with or without 2 mM MnCl₂ in the presence of 20% PEG-10000 (w/v). The mixed solution was transferred to a 96-well plate and visualized with a 60 \times oil immersion objective under a Nikon A1 microscope (Nikon Corporation).

Fluorescence recovery after photobleaching (FRAP) assay

For each FRAP measurement, 5 μ l of the fluorescence-labeled α -Syn condensates were dropped onto a glass slide. The sample was then covered with a 12 mm coverslip, sealed with nail paint, and dried with nitrogen. FRAP was performed using a Nikon A1 microscope, and the measurements involved two prebleaching frames, one flash of bleaching (100% of laser power), and six postbleaching frames. For EGFP-labeled and rhodamine-labeled α -Syn condensates, photo-bleaching was carried out using a 488 nm and 561 nm laser, respectively. Data were normalized to the maximal prebleach and minimal postbleach fluorescence intensities.

Sedimentation-based assay

Sedimentation and electrophoresis assays were performed as previously described (83). Each α -Syn sample contains 200 μ M α -Syn with a total volume of 50 μ l. The phase-separated α -Syn protein in each sample was separated by centrifugation at 16,000g for 10 min. The supernatant was collected, and the pellet was washed and resuspended with 50 μ l of the same buffer. The same volume of samples from supernatant and pellet were analyzed by SDS-PAGE.

Turbidity assay

The turbidity was employed to evaluate the protein phase separation. The samples were added to a transparent 96-well plate in a turbidity assay, and the absorbance at 405 nm was measured at 37 $^{\circ}$ C using a BioTek Synergy HT microplate reader (80). Full accounting of statistical significance was included for each figure based on at least three independent experiments.

Thioflavin T (ThT) fluorescence

The formation of α -Syn amyloid aggregates was monitored using a ThT assay as previously described (70). Briefly, all α -Syn samples were diluted to 5 μ M, and the final concentration of ThT is 40 μ M. Fluorescence was measured on a BioTek Synergy HT microplate reader. The excitation wavelength was 440 nm and the emission intensity at 485 nm was used for analysis. Full accounting of statistical significance was included for each figure based on at least three independent experiments.

Thioflavin S (ThS) staining assay

ThS solution was prepared at a concentration of 0.0625% in protein storage buffer. For each sample, 10 μ l of α -Syn condensates was incubated with 1 μ l ThS solution at 37 $^{\circ}$ C for 12 h. ThS fluorescence was visualized under a Nikon A1 microscope with a 60 \times oil immersion objective lens.

Liposome preparation

All lipids used in this work were acquired from Avanti Polar Lipids Inc. 1-palmitoyl-2-oleoyl-glycero-3-phosphocholine (POPC, CAT#850457C), 1-palmitoyl-2-oleoyl-sn-glycero-3-phospho-L-serine (POPS, CAT#840034C), 1,2-dipalmitoyl-sn-glycero-3-phosphoethanolamine-N-(lissamine rhodamine B sulfonyl) (Rhod PE, CAT#810158P) were mixed at the molar ratio of 84.5:15:0.5. After evaporation by nitrogen, the lipids were dried and resuspended in the reconstitution buffer (25 mM Tris-HCl [pH7.4], 50 mM NaCl) (81, 84). The resuspended lipid bilayers were then performed six freeze-thaw cycles using liquid nitrogen followed by extrusion through 50 nm pore size filters using a miniextruder (Avanti Polar Lipids).

Transmission electron microscopy

α -Syn protein with or without MnCl₂ agitated at 37 °C for 113 h. The samples were dropped on the carbon-coated copper grids and subsequently stained with 2% uranyl acetate (84). EM images were observed on an H-7650 TEM (HITACHI) at 80 kv of acceleration voltage.

Cell culture and MTT assay

PC12 cells were cultured in high-glucose DMEM (WISENT INC) supplemented with 10% FBS, 5% Donor Equine Serum (HyClone), 100 units/ml of penicillin, and 100 μ g/ml of streptomycin in a water-saturated atmosphere of 5% CO₂ at 37 °C (83). Cells were seeded in 96-well microtiter plates at 5 \times 10³ cells/well in 100 μ l medium and incubated for 12 h. PC12 cells were treated with PBS, α -Syn monomers, Mn²⁺, Mn²⁺/ α -Syn condensates, α -Syn fibrils, Mn²⁺/ α -Syn fibrils, respectively. After 24 h, 10 μ l MTT (5 μ g/ml, prepared in PBS) was added, and the cells were continued to culture for another 4 h. The medium was removed, and 150 μ l of dimethyl sulfoxide (DMOS) was added to each well. After 10 min, the absorption at 490 nm was measured by a BioTek Synergy HT microplate reader.

Statistical analysis

All data are presented as the mean \pm SD and were analyzed using GraphPad Prism 8.0.2 software for Windows. Statistical significance was calculated using one-way ANOVA, and *p* value <0.05 was considered as statistically significant.

Data availability

All data presented are contained within the main manuscript and supporting information.

Supporting information—This article contains supporting information.

Acknowledgments—We thank Dr Jingshi Shen, Tao Gao for insightful discussions and Xiaojun Wang for technical assistance. This work was supported by the National Natural Science Foundation of China (NSFC) grants (Nos. 91854117, 31871425, and

32100546), Natural Science Foundation of Jiangsu Province (BK20200036), the Priority Academic Program Development of Jiangsu Higher Education Institutions (PAPD), Six Talent Peaks Project in Jiangsu Province, and Jiangsu Distinguished Professor Funding.

Author contributions—Y. L., D. W., and H. Y. conceptualization; B. X. data curation; C. W. formal analysis; B. X., S. H., and Y. L. investigation; C. W. and Y. G. methodology; D. W. and H. Y. supervision; B. X., Y. L., and H. Y. writing—original draft.

Conflict of interest—The authors declare that they have no conflicts of interest with the contents of this article.

Abbreviations—The abbreviations used are: α -Syn, α -synuclein; FRAP, fluorescence recovery after photobleaching; IDR, intrinsically disordered region; LLPS, liquid-liquid phase separation; PD, Parkinson's disease; ThS, thioflavin S; ThT, thioflavin T.

References

- Baba, M., Nakajo, S., Tu, P. H., Tomita, T., Nakaya, K., Lee, V. M., Trojanowski, J. Q., and Iwatsubo, T. (1998) Aggregation of alpha-synuclein in Lewy bodies of sporadic Parkinson's disease and dementia with Lewy bodies. *Am. J. Pathol.* **152**, 879–884
- Maroteaux, L., Campanelli, J. T., and Scheller, R. H. (1988) Synuclein: A neuron-specific protein localized to the nucleus and presynaptic nerve terminal. *J. Neurosci.* **8**, 2804–2815
- Bernal-Conde, L. D., Ramos-Acevedo, R., Reyes-Hernández, M. A., Balbuena-Olvera, A. J., Morales-Moreno, I. D., Argüero-Sánchez, R., Schüle, B., and Guerra-Crespo, M. (2019) Alpha-synuclein physiology and pathology: A perspective on cellular structures and organelles. *Front. Neurosci.* **13**, 1399
- Fauvet, B., Mbefo, M. K., Fares, M. B., Desobry, C., Michael, S., Ardah, M. T., Tsika, E., Coune, P., Prudent, M., Lion, N., Eliezer, D., Moore, D. J., Schneider, B., Aebischer, P., El-Agnaf, O. M., et al. (2012) α -Synuclein in central nervous system and from erythrocytes, mammalian cells, and Escherichia coli exists predominantly as disordered monomer. *J. Biol. Chem.* **287**, 15345–15364
- Theillet, F. X., Binolfi, A., Bekei, B., Martorana, A., Rose, H. M., Stuijver, M., Verzini, S., Lorenz, D., van Rossum, M., Goldfarb, D., and Selenko, P. (2016) Structural disorder of monomeric α -synuclein persists in mammalian cells. *Nature* **530**, 45–50
- Nguyen, P. H., and Derreumaux, P. (2020) Structures of the intrinsically disordered A β , tau and α -synuclein proteins in aqueous solution from computer simulations. *Biophys. Chem.* **264**, 106421
- Bartels, T., Choi, J. G., and Selkoe, D. J. (2011) α -Synuclein occurs physiologically as a helically folded tetramer that resists aggregation. *Nature* **477**, 107–110
- Wang, W., Perovic, I., Chittuluru, J., Kaganovich, A., Nguyen, L. T., Liao, J., Auclair, J. R., Johnson, D., Landeru, A., Simorellis, A. K., Ju, S., Cookson, M. R., Asturias, F. J., Agar, J. N., Webb, B. N., et al. (2011) A soluble α -synuclein construct forms a dynamic tetramer. *Proc. Natl. Acad. Sci. U. S. A.* **108**, 17797–17802
- Burré, J., Sharma, M., Tsetsenis, T., Buchman, V., Etherton, M. R., and Südhof, T. C. (2010) Alpha-synuclein promotes SNARE-complex assembly *in vivo* and *in vitro*. *Science* **329**, 1663–1667
- Nguyen, P. H., Ramamoorthy, A., Sahoo, B. R., Zheng, J., Faller, P., Straub, J. E., Dominguez, L., Shea, J. E., Dokholyan, N. V., De Simone, A., Ma, B., Nussinov, R., Najafi, S., Ngo, S. T., Loquet, A., et al. (2021) Amyloid oligomers: A joint experimental/computational perspective on Alzheimer's disease, Parkinson's disease, type II diabetes, and amyotrophic lateral sclerosis. *Chem. Rev.* **121**, 2545–2647
- Agerschou, E. D., Schützmann, M. P., Reppert, N., Wördehoff, M. M., Shaykhalishahi, H., Buell, A. K., and Hoyer, W. (2021) β -Turn exchanges

Mn²⁺-induced α -synuclein phase transition

- in the α -synuclein segment 44-TKEG-47 reveal high sequence fidelity requirements of amyloid fibril elongation. *Biophys. Chem.* **269**, 106519
12. Spillantini, M. G., Schmidt, M. L., Lee, V. M., Trojanowski, J. Q., Jakes, R., and Goedert, M. (1997) α -Synuclein in Lewy bodies. *Nature* **388**, 839–840
 13. Nemani, V. M., Lu, W., Berge, V., Nakamura, K., Onoa, B., Lee, M. K., Chaudhry, F. A., Nicoll, R. A., and Edwards, R. H. (2010) Increased expression of α -synuclein reduces neurotransmitter release by inhibiting synaptic vesicle recluster after endocytosis. *Neuron* **65**, 66–79
 14. Karpinar, D. P., Balija, M. B., Kügler, S., Opazo, F., Rezaei-Ghaleh, N., Wender, N., Kim, H. Y., Taschenberger, G., Falkenburger, B. H., Heise, H., Kumar, A., Riedel, D., Fichtner, L., Voigt, A., Braus, G. H., *et al.* (2009) Pre-fibrillar α -synuclein variants with impaired beta-structure increase neurotoxicity in Parkinson's disease models. *EMBO J.* **28**, 3256–3268
 15. Volpicelli-Daley, L. A., Luk, K. C., Patel, T. P., Tanik, S. A., Riddle, D. M., Stieber, A., Meaney, D. F., Trojanowski, J. Q., and Lee, V. M. (2011) Exogenous α -synuclein fibrils induce Lewy body pathology leading to synaptic dysfunction and neuron death. *Neuron* **72**, 57–71
 16. Fields, C. R., Bengoa-Vergniory, N., and Wade-Martins, R. (2019) Targeting α -synuclein as a therapy for Parkinson's disease. *Front. Mol. Neurosci.* **12**, 299
 17. Wong, Y. C., and Krainc, D. (2017) α -Synuclein toxicity in neurodegeneration: Mechanism and therapeutic strategies. *Nat. Med.* **23**, 1–13
 18. Guiney, S. J., Adlard, P. A., Lei, P., Mawal, C. H., Bush, A. I., Finkelstein, D. I., and Ayton, S. (2020) Fibrillar α -synuclein toxicity depends on functional lysosomes. *J. Biol. Chem.* **295**, 17497–17513
 19. Nguyen, P. H., Sterpone, F., Pouplana, R., Derreumaux, P., and Campanera, J. M. (2016) Dimerization mechanism of Alzheimer A β (40) peptides: The high content of intrapeptide-stabilized conformations in A2V and A2T heterozygous dimers retards amyloid fibril formation. *J. Phys. Chem. B* **120**, 12111–12126
 20. Ivanova, M. I., Lin, Y., Lee, Y. H., Zheng, J., and Ramamoorthy, A. (2021) Biophysical processes underlying cross-seeding in amyloid aggregation and implications in amyloid pathology. *Biophys. Chem.* **269**, 106507
 21. Doig, A. J., and Derreumaux, P. (2015) Inhibition of protein aggregation and amyloid formation by small molecules. *Curr. Opin. Struct. Biol.* **30**, 50–56
 22. Savitt, D., and Jankovic, J. (2019) Targeting α -synuclein in Parkinson's disease: Progress towards the development of disease-modifying therapeutics. *Drugs* **79**, 797–810
 23. Shahmoradian, S. H., Lewis, A. J., Genoud, C., Hench, J., Moors, T. E., Navarro, P. P., Castaño-Diez, D., Schweighauser, G., Graff-Meyer, A., Goldie, K. N., Sütterlin, R., Huisman, E., Ingrassia, A., Gier, Y., Roze-muller, A. J. M., *et al.* (2019) Lewy pathology in Parkinson's disease consists of crowded organelles and lipid membranes. *Nat. Neurosci.* **22**, 1099–1109
 24. Muñoz, S. S., Petersen, D., Marlet, F. R., Kücükköse, E., and Galvagnion, C. (2021) The interplay between glucocerebrosidase, α -synuclein and lipids in human models of Parkinson's disease. *Biophys. Chem.* **273**, 106534
 25. Watson, M. D., Flynn, J. D., and Lee, J. C. (2021) Raman spectral imaging of (13)C(2)H(15)N-labeled α -synuclein amyloid fibrils in cells. *Biophys. Chem.* **269**, 106528
 26. Galvagnion, C., Buell, A. K., Meisl, G., Michaels, T. C., Vendruscolo, M., Knowles, T. P., and Dobson, C. M. (2015) Lipid vesicles trigger α -synuclein aggregation by stimulating primary nucleation. *Nat. Chem. Biol.* **11**, 229–234
 27. Giehm, L., Svergun, D. I., Otzen, D. E., and Vestergaard, B. (2011) Low-resolution structure of a vesicle disrupting α -synuclein oligomer that accumulates during fibrillation. *Proc. Natl. Acad. Sci. U. S. A.* **108**, 3246–3251
 28. Kurochka, A. S., Yushchenko, D. A., Bouř, P., and Shvadchak, V. V. (2021) Influence of lipid membranes on α -synuclein aggregation. *ACS Chem. Neurosci.* **12**, 825–830
 29. González, N., Arcos-López, T., König, A., Quintanar, L., Menacho Márquez, M., Outeiro, T. F., and Fernández, C. O. (2019) Effects of α -synuclein post-translational modifications on metal binding. *J. Neurochem.* **150**, 507–521
 30. Binolfi, A., Rasia, R. M., Bertoncini, C. W., Ceolin, M., Zweckstetter, M., Griesinger, C., Jovin, T. M., and Fernández, C. O. (2006) Interaction of α -synuclein with divalent metal ions reveals key differences: A link between structure, binding specificity and fibrillation enhancement. *J. Am. Chem. Soc.* **128**, 9893–9901
 31. Pfalzer, A. C., and Bowman, A. B. (2017) Relationships between essential manganese biology and manganese toxicity in neurological disease. *Curr. Environ. Health Rep.* **4**, 223–228
 32. Tinkov, A. A., Paoliello, M. M. B., Mazilina, A. N., Skalny, A. V., Martins, A. C., Voskresenskaya, O. N., Aaseth, J., Santamaria, A., Notova, S. V., Tsatsakis, A., Lee, E., Bowman, A. B., and Aschner, M. (2021) Molecular targets of manganese-induced neurotoxicity: A five-year update. *Int. J. Mol. Sci.* **22**, 4646
 33. Guilarte, T. R. (2013) Manganese neurotoxicity: New perspectives from behavioral, neuroimaging, and neuropathological studies in humans and non-human primates. *Front. Aging Neurosci.* **5**, 23
 34. Miah, M. R., Ijomone, O. M., Okoh, C. O. A., Ijomone, O. K., Akingbade, G. T., Ke, T., Krum, B., da Cunha Martins, A., Jr., Akinyemi, A., Aranoff, N., Antunes Soares, F. A., Bowman, A. B., and Aschner, M. (2020) The effects of manganese overexposure on brain health. *Neurochem. Int.* **135**, 104688
 35. Gorell, J. M., Johnson, C. C., Rybicki, B. A., Peterson, E. L., Kortsha, G. X., Brown, G. G., and Richardson, R. J. (1999) Occupational exposure to manganese, copper, lead, iron, mercury and zinc and the risk of Parkinson's disease. *Neurotoxicology* **20**, 239–247
 36. Lucchini, R. G., Martin, C. J., and Doney, B. C. (2009) From manganism to manganese-induced parkinsonism: A conceptual model based on the evolution of exposure. *Neuromolecular Med.* **11**, 311–321
 37. Racette, B. A., McGee-Minnich, L., Moerlein, S. M., Mink, J. W., Videen, T. O., and Perlmutter, J. S. (2001) Welding-related parkinsonism: Clinical features, treatment, and pathophysiology. *Neurology* **56**, 8–13
 38. Jiang, Y. M., Mo, X. A., Du, F. Q., Fu, X., Zhu, X. Y., Gao, H. Y., Xie, J. L., Liao, F. L., Pira, E., and Zheng, W. (2006) Effective treatment of manganese-induced occupational parkinsonism with p-aminosalicylic acid: A case of 17-year follow-up study. *J. Occup. Environ. Med.* **48**, 644–649
 39. Racette, B. A., Tabbal, S. D., Jennings, D., Good, L., Perlmutter, J. S., and Evanoff, B. (2005) Prevalence of parkinsonism and relationship to exposure in a large sample of Alabama welders. *Neurology* **64**, 230–235
 40. Rutchik, J. S., Zheng, W., Jiang, Y., and Mo, X. (2012) How does an occupational neurologist assess welders and steelworkers for a manganese-induced movement disorder? An international team's experiences in Guanxi, China part II. *J. Occup. Environ. Med.* **54**, 1562–1564
 41. Rutchik, J. S., Zheng, W., Jiang, Y., and Mo, X. (2012) How does an occupational neurologist assess welders and steelworkers for a manganese-induced movement disorder? An international team's experiences in Guanxi, China, part I. *J. Occup. Environ. Med.* **54**, 1432–1434
 42. Racette, B. A., Criswell, S. R., Lundin, J. I., Hobson, A., Seixas, N., Kotzbauer, P. T., Evanoff, B. A., Perlmutter, J. S., Zhang, J., Sheppard, L., and Checkoway, H. (2012) Increased risk of parkinsonism associated with welding exposure. *Neurotoxicology* **33**, 1356–1361
 43. Mortimer, J. A., Borenstein, A. R., and Nelson, L. M. (2012) Associations of welding and manganese exposure with Parkinson disease: Review and meta-analysis. *Neurology* **79**, 1174–1180
 44. Al-Lozi, A., Nielsen, S. S., Hershey, T., Birke, A., Checkoway, H., Criswell, S. R., and Racette, B. A. (2017) Cognitive control dysfunction in workers exposed to manganese-containing welding fume. *Am. J. Ind. Med.* **60**, 181–188
 45. Bowler, R. M., Kornblith, E. S., Gocheva, V. V., Colledge, M. A., Bollweg, G., Kim, Y., Beseler, C. L., Wright, C. W., Adams, S. W., and Lobdell, D. T. (2015) Environmental exposure to manganese in air: Associations with cognitive functions. *Neurotoxicology* **49**, 139–148
 46. Carvalho, C. F., Oulhote, Y., Martorelli, M., Carvalho, C. O., Menezes-Filho, J. A., Argollo, N., and Abreu, N. (2018) Environmental manganese

- exposure and associations with memory, executive functions, and hyperactivity in Brazilian children. *Neurotoxicology* **69**, 253–259
47. Du, K., Liu, M. Y., Pan, Y. Z., Zhong, X., and Wei, M. J. (2018) Association of circulating manganese levels with Parkinson's disease: A meta-analysis. *Neurosci. Lett.* **665**, 92–98
 48. Sun, Y., He, Y., Yang, L., Liang, D., Shi, W., Zhu, X., Jiang, Y., and Ou, C. (2020) Manganese induced nervous injury by α -synuclein accumulation via ATP-sensitive K(+) channels and GABA receptors. *Toxicol. Lett.* **332**, 164–170
 49. Liu, Z. Q., Liu, K., Liu, Z. F., Cong, L., Lei, M. Y., Ma, Z., Li, J., Deng, Y., Liu, W., and Xu, B. (2021) Manganese-induced α -synuclein overexpression aggravates mitochondrial damage by repressing PINK1/parkin-mediated mitophagy. *Food Chem. Toxicol.* **152**, 112213
 50. Verina, T., Schneider, J. S., and Guilarte, T. R. (2013) Manganese exposure induces α -synuclein aggregation in the frontal cortex of non-human primates. *Toxicol. Lett.* **217**, 177–183
 51. Cai, T., Yao, T., Zheng, G., Chen, Y., Du, K., Cao, Y., Shen, X., Chen, J., and Luo, W. (2010) Manganese induces the overexpression of α -synuclein in PC12 cells via ERK activation. *Brain Res.* **1359**, 201–207
 52. Harischandra, D. S., Rokad, D., Neal, M. L., Ghaisas, S., Manne, S., Sarkar, S., Panicker, N., Zenitsky, G., Jin, H., Lewis, M., Huang, X., Anantharam, V., Kanthasamy, A., and Kanthasamy, A. G. (2019) Manganese promotes the aggregation and prion-like cell-to-cell exosomal transmission of α -synuclein. *Sci. Signal.* **12**, eaau4543
 53. Han, J. Y., Choi, T. S., and Kim, H. I. (2018) Molecular role of Ca(2+) and hard divalent metal cations on accelerated fibrillation and interfibrillar aggregation of α -synuclein. *Sci. Rep.* **8**, 1895
 54. Li, P., Banjade, S., Cheng, H. C., Kim, S., Chen, B., Guo, L., Llaguno, M., Hollingsworth, J. V., King, D. S., Banani, S. F., Russo, P. S., Jiang, Q. X., Nixon, B. T., and Rosen, M. K. (2012) Phase transitions in the assembly of multivalent signalling proteins. *Nature* **483**, 336–340
 55. Conicella, A. E., Dignon, G. L., Zerze, G. H., Schmidt, H. B., D'Ordine, A. M., Kim, Y. C., Rohatgi, R., Ayala, Y. M., Mittal, J., and Fawzi, N. L. (2020) TDP-43 α -helical structure tunes liquid-liquid phase separation and function. *Proc. Natl. Acad. Sci. U. S. A.* **117**, 5883–5894
 56. Levone, B. R., Lenzken, S. C., Antonaci, M., Maiser, A., Rapp, A., Conte, F., Reber, S., Mechttersheimer, J., Ronchi, A. E., Mühlemann, O., Leonhardt, H., Cardoso, M. C., Ruepp, M. D., and Barabino, S. M. L. (2021) FUS-dependent liquid-liquid phase separation is important for DNA repair initiation. *J. Cell Biol.* **220**, e202008030
 57. Ambadipudi, S., Biernat, J., Riedel, D., Mandelkow, E., and Zweckstetter, M. (2017) Liquid-liquid phase separation of the microtubule-binding repeats of the Alzheimer-related protein tau. *Nat. Commun.* **8**, 275
 58. Wegmann, S., Eftekharzadeh, B., Tepper, K., Zoltowska, K. M., Bennett, R. E., Dujardin, S., Laskowski, P. R., MacKenzie, D., Kamath, T., Commins, C., Vanderburg, C., Roe, A. D., Fan, Z., Molliex, A. M., Hernandez-Vega, A., et al. (2018) Tau protein liquid-liquid phase separation can initiate tau aggregation. *EMBO J.* **37**, e98049
 59. Tange, H., Ishibashi, D., Nakagaki, T., Taguchi, Y., Kamatari, Y. O., Ozawa, H., and Nishida, N. (2021) Liquid-liquid phase separation of full-length prion protein initiates conformational conversion *in vitro*. *J. Biol. Chem.* **296**, 100367
 60. Pytowski, L., Lee, C. F., Foley, A. C., Vaux, D. J., and Jean, L. (2020) Liquid-liquid phase separation of type II diabetes-associated IAPP initiates hydrogelation and aggregation. *Proc. Natl. Acad. Sci. U. S. A.* **117**, 12050–12061
 61. Xing, Y., Nandakumar, A., Kakinen, A., Sun, Y., Davis, T. P., Ke, P. C., and Ding, F. (2021) Amyloid aggregation under the lens of liquid-liquid phase separation. *J. Phys. Chem. Lett.* **12**, 368–378
 62. Ray, S., Singh, N., Kumar, R., Patel, K., Pandey, S., Datta, D., Mahato, J., Panigrahi, R., Navalkar, A., Mehra, S., Gadhe, L., Chatterjee, D., Sawner, A. S., Maiti, S., Bhatia, S., et al. (2020) α -Synuclein aggregation nucleates through liquid-liquid phase separation. *Nat. Chem.* **12**, 705–716
 63. Hardenberg, M. C., Sinnige, T., Casford, S., Dada, S., Poudel, C., Robinson, E. A., Fuxreiter, M., Kaminski, C., Kaminski-Schierle, G. S., Nollen, E. A. A., Dobson, C. M., and Vendruscolo, M. (2021) Observation of an α -synuclein liquid droplet state and its maturation into Lewy body-like assemblies. *J. Mol. Cell Biol.* **13**, 282–294
 64. Hoffmann, C., Sansevino, R., Morabito, G., Logan, C., Vabulas, R. M., Ulusoy, A., Ganzella, M., and Milovanovic, D. (2021) Synapsin condensates recruit α -synuclein. *J. Mol. Biol.* **433**, 166961
 65. Man, W. K., Tahirbegi, B., Vrettas, M. D., Preet, S., Ying, L., Vendruscolo, M., De Simone, A., and Fusco, G. (2021) The docking of synaptic vesicles on the presynaptic membrane induced by α -synuclein is modulated by lipid composition. *Nat. Commun.* **12**, 927
 66. Perrin, R. J., Woods, W. S., Clayton, D. F., and George, J. M. (2000) Interaction of human α -synuclein and Parkinson's disease variants with phospholipids. Structural analysis using site-directed mutagenesis. *J. Biol. Chem.* **275**, 34393–34398
 67. Fusco, G., De Simone, A., Gopinath, T., Vostrikov, V., Vendruscolo, M., Dobson, C. M., and Veglia, G. (2014) Direct observation of the three regions in α -synuclein that determine its membrane-bound behaviour. *Nat. Commun.* **5**, 3827
 68. Boyko, S., Qi, X., Chen, T. H., Surewicz, K., and Surewicz, W. K. (2019) Liquid-liquid phase separation of tau protein: The crucial role of electrostatic interactions. *J. Biol. Chem.* **294**, 11054–11059
 69. Wu, X., Cai, Q., Shen, Z., Chen, X., Zeng, M., Du, S., and Zhang, M. (2019) RIM and RIM-BP form presynaptic active-zone-like condensates via phase separation. *Mol. Cell* **73**, 971–984.e5
 70. LeVine, H., 3rd (1993) Thioflavine T interaction with synthetic Alzheimer's disease beta-amyloid peptides: Detection of amyloid aggregation in solution. *Protein Sci.* **2**, 404–410
 71. Fusco, G., Chen, S. W., Williamson, P. T. F., Cascella, R., Perni, M., Jarvis, J. A., Cecchi, C., Vendruscolo, M., Chiti, F., Cremades, N., Ying, L., Dobson, C. M., and De Simone, A. (2017) Structural basis of membrane disruption and cellular toxicity by α -synuclein oligomers. *Science* **358**, 1440–1443
 72. Li, C. H., Coffey, E. L., Dall'Agnesse, A., Hannett, N. M., Tang, X., Henninger, J. E., Platt, J. M., Oksuz, O., Zamudio, A. V., Afeyan, L. K., Schuijers, J., Liu, X. S., Markoulaki, S., Lungiangwa, T., LeRoy, G., et al. (2020) MeCP2 links heterochromatin condensates and neurodevelopmental disease. *Nature* **586**, 440–444
 73. Hernández-Vega, A., Braun, M., Scharrel, L., Jahnel, M., Wegmann, S., Hyman, B. T., Alberti, S., Diez, S., and Hyman, A. A. (2017) Local nucleation of microtubule bundles through tubulin concentration into a condensed tau phase. *Cell Rep.* **20**, 2304–2312
 74. Gasset-Rosa, F., Lu, S., Yu, H., Chen, C., Melamed, Z., Guo, L., Shorter, J., Da Cruz, S., and Cleveland, D. W. (2019) Cytoplasmic TDP-43 de-mixing independent of stress granules drives inhibition of nuclear import, loss of nuclear TDP-43, and cell death. *Neuron* **102**, 339–357.e7
 75. Peres, T. V., Parmalee, N. L., Martinez-Finley, E. J., and Aschner, M. (2016) Untangling the manganese- α -synuclein web. *Front. Neurosci.* **10**, 364
 76. Pujols, J., Peña-Díaz, S., Pallarès, I., and Ventura, S. (2020) Chemical chaperones as novel drugs for Parkinson's disease. *Trends Mol. Med.* **26**, 408–421
 77. Babinchak, W. M., Dumm, B. K., Venus, S., Boyko, S., Putnam, A. A., Jankowsky, E., and Surewicz, W. K. (2020) Small molecules as potent biphasic modulators of protein liquid-liquid phase separation. *Nat. Commun.* **11**, 5574
 78. Pradhan, A., Mishra, S., Surolia, A., and Panda, D. (2021) C1 inhibits liquid-liquid phase separation and oligomerization of tau and protects neuroblastoma cells against toxic tau oligomers. *ACS Chem. Neurosci.* **12**, 1989–2002
 79. Yu, H., Rathore, S. S., Shen, C., Liu, Y., Ouyang, Y., Stowell, M. H., and Shen, J. (2015) Reconstituting intracellular vesicle fusion reactions: The essential role of macromolecular crowding. *J. Am. Chem. Soc.* **137**, 12873–12883
 80. Qian, T., Li, C., He, R., Wan, C., Liu, Y., and Yu, H. (2021) Calcium-dependent and -independent lipid transfer mediated by tricalbins in yeast. *J. Biol. Chem.* **296**, 100729

Mn²⁺-induced α -synuclein phase transition

81. Liu, Y., Wan, C., Rathore, S. S., Stowell, M. H. B., Yu, H., and Shen, J. (2021) SNARE zippering is suppressed by a conformational constraint that is removed by v-SNARE splitting. *Cell Rep.* **34**, 108611
82. Yu, H., Shen, C., Liu, Y., Menasche, B. L., Ouyang, Y., Stowell, M. H. B., and Shen, J. (2018) SNARE zippering requires activation by SNARE-like peptides in Sec1/Munc18 proteins. *Proc. Natl. Acad. Sci. U. S. A.* **115**, E8421–e8429
83. Yu, H., Li, M., Liu, G., Geng, J., Wang, J., Ren, J., Zhao, C., and Qu, X. (2012) Metallosupramolecular complex targeting an α/β discordant stretch of amyloid β peptide. *Chem. Sci.* **3**, 3145–3153
84. Yu, H., Rathore, S. S., Davis, E. M., Ouyang, Y., and Shen, J. (2013) Doc2b promotes GLUT4 exocytosis by activating the SNARE-mediated fusion reaction in a calcium- and membrane bending-dependent manner. *Mol. Biol. Cell* **24**, 1176–1184